Received: 28 December 2022 | Revised: 16 September 2023 | Accepted: 20 September 2023

DOI: 10.1002/bio.4602

LUMINESCENCE WILEY
The Journal of Biological and Chemical Luminescence

RESEARCH ARTICLE

Mechanoluminescence and photoluminescence properties of Eu^{3+}-activated $SrGa_2O_4$ phosphors

Baby Vasanthi[1,2] | Narayana Panickar Gopakumar[2] | Prabhakaran Sreekumari Anjana[1] | Girija Nair[1,3]

[1]Post Graduate Department of Physics, All Saints' College, University of Kerala, Thiruvananthapuram, Kerala, India

[2]Post Graduate Department of Physics and Research Centre, Mahatma Gandhi College, University of Kerala, Thiruvananthapuram, India

[3]Post Graduate Department of Physics, NSS College, Pandalam, University of Kerala, Pathanamthitta, India

Correspondence
Prabhakaran Sreekumari Anjana, Post Graduate Department of Physics, All Saints' College, University of Kerala, Thiruvananthapuram 695007, Kerala, India.
Email: psanjanaa@yahoo.com

Funding information
Aspire Fellowship, Department of Collegiate Education, Government of Kerala

Abstract

Red-emitting Eu^{3+} activated $SrGa_2O_4$ phosphors were synthesized using a conventional solid-state reaction method. The structural, optical, and luminescence properties were systematically investigated. The synthesized phosphors are single phase with a monoclinic structure. There are no significant changes in the phase and the crystal structure of the host matrix after incorporating Eu^{3+} ions. The undoped and Eu^{3+} doped $SrGa_2O_4$ phosphors exhibited good mechanoluminescence (ML) emission without any irradiation with ultraviolet (UV) or gamma rays. Eu^{3+}-activated $SrGa_2O_4$ phosphors have prominent red emission attributed to $^5D_0 \rightarrow {}^7F_2$ forced electric dipole transition excited at 395 nm. The colour coordinates and purity of the $SrGa_2O_4$: 0.08 Eu^{3+} phosphor were calculated to be (0.6102, 0.3810) and 97.6%, respectively. The quantum efficiency is 12.68%, and was better than that of commercially available red phosphors. The ML and photoluminescence studies revealed that the synthesized phosphors can act as potential candidates for stress sensors, UV or near-UV light-emitting diodes (NUV LEDs) and components of phosphor-converted white light-emitting diode (pc-WLED) applications.

KEYWORDS
gallates, lifetime, mechanoluminescence, photoluminescence, X-ray diffraction

1 | INTRODUCTION

The materials capable of exhibiting light emissions are luminescent or phosphors. Luminescence can be divided into various categories such as photoluminescence (PL), electroluminescence (EL), cathodoluminescence (CL), mechanoluminescence (ML) and so forth, depending on the excitation source used [1]. Among these, ML attained a specific attraction in the current research field due to its ability to show visible light emission under different mechanical actions performed in the samples. ML is the form of luminescence induced using mechanical processes such as grinding, rubbing, cutting, cleaving, shaking, scratching, compressing or impulsive crushing on solid materials [2]. ML is a phenomenon that has long been known to human civilization; Bacon mentioned it in the earliest document with clear evidence in 1605 [3]. The technological applications of ML materials were scarcely reported in the literature before 1990s due to poor ML emissions from the materials.

In recent years, the research field has imparted emphasis to ML materials in the areas of lighting devices, damage, and impact sensors, aerospace engineering, smart robotics, biomedicine, sensors for stress indicators, visualizations of stress distribution in solids and wireless fracture sensor systems and so forth [4,5]. The development in science and technology provides immense opportunities for scientists and engineers to synthesize and develop ML materials with excellent emission intensity and whose ML emission can be seen in daylight with the naked eye [6,7]. The recoverability, wireless detection, powerful light emission and nondestructive examination are only a few of the unusual qualities of ML materials [8]. ML materials with a linear relationship between ML intensity and impact load in the elastic deformation region reliably allow real-time detection signals of stress

[8,9]. ML is generally associated with a trap-involved process. During this process, electrons or holes are kept for a while in the trap centres, and then they recombine with the luminescence centre either by travelling in the conduction band or valence band or by electron tunnelling [10].

ML can be divided into deformation luminescence and triboluminescence in accordance with the physical processes involved. Deformation ML is a kind of ML that arises when materials emit light due to mechanical deformation. It involves the generation of light as a direct result of applied stress, such as stretching, twisting or compressing a material [8]. The phenomenon of deformation ML has been observed in various materials, including crystals, polymers, and composites. When these materials experience deformation, the internal structure undergoes changes, causing the release of stored energy in the form of light. The emitted light can range from visible to ultraviolet (UV) or infrared, depending on the specific material [11]. Deformation luminescence can be further categorized into elastico ML, plastico ML and fracto-ML based on the deformation approach that occurs in materials for the emission of light [8,11]. Applications for deformation ML include stress sensing, structural monitoring and material characterization [7]. Triboluminescence emerges from triboelectricity, tribochemical reactions and tribothermalization originating from the contact and the separation of two dissimilar materials, respectively [7,8]. Triboluminescence involves light emission resulting from the fracture or rubbing of materials. Triboluminescent materials typically involve the breaking of crystal lattices, resulting in the release of stored energy in the form of light [12]. Depending on the material and the strength of the mechanical forces involved, the produced light can range from a faint glow to apparent sparks or flashes [4]. Some of the trivial limitations reported on ML materials are their weak ML intensity, limited ML colour and the possibility of structural damage in the ML materials due to the impact of stress applied to it and so on [11].

The intense red emission of Eu^{3+} activated $SrGa_2O_4$ phosphors is caused by the predominating hypersensitive electric dipole (ED) $^5D_0 \rightarrow {}^7F_2$ transitions, which makes this phosphor a good candidate for use in solid-state light-emitting devices, near-UV light-emitting diodes (NUV LEDs), biomedical probes, field emission display channels and phosphor-converted white light-emitting diode (pc-WLED) applications [12,13]. The luminescence in Eu^{3+}-doped AB_2O_4 (A = Sr, B = Al, Gd) spinel structures has been extensively reported as a result of its vast applications in display devices and white light-emitting diodes. The authors Ayvacıklı *et al*. have investigated the structural and optical details of Eu^{3+}-doped $SrAl_2O_4$ phosphors [14]. Jamalaiah and Jayasimhadri studied the tunable luminescence properties of $SrAl_2O_4$:Eu^{3+} phosphors for LED applications [15]. Jha and Kharea investigated the applications of $SrAl_2O_4$:Eu, Dy phosphors in mechanoluminescent flexible film for impact sensors [7]. In 2020, Ashwini *et al*. reported the near-UV light-excitable $SrAl_2O_4$:Eu^{3+} nanophosphors for display device applications [16]. Chaware and Rewatkar studied the structural and PL study of $SrAl_2O_4$:Eu^{3+} phosphors [17]. De *et al*. attempted to describe enhanced red PL in chain-like $SrAl_2O_4$:Eu^{3+} nanophosphors [18]. Wang *et al*. investigated the red luminescence from Eu^{3+}-doped $SrGd_2O_4$ phosphors and reported the relationship between the emission intensities and Eu^{3+} concentrations [19]. However, only few studies have reported Eu^{3+}-activated $SrGa_2O_4$ phosphors. Cai *et al*. reported the luminescence studies of Eu^{3+}-activated $SrGa_2O_4$ phosphors [13].

The ML of gallate-based systems has been barely reported. Several authors have reported the ML properties of aluminates and silicates, especially the ML of $SrAl_2O_4$ phosphors doped with rare earth ions [4–8]. To the best of our knowledge, the ML of the $SrGa_2O_4$ phosphor activated with rare earth ions has not been reported until now. In this work, an effort was made to study the ML properties of Eu^{3+}-activated $SrGa_2O_4$ phosphors for the first time without any irradiation of UV or gamma rays. The effect of Eu^{3+} concentration and impact velocity on the intensity of the ML glow curve has been investigated. The synthesized phosphors have both ML and PL properties making them suitable for use in pc-WLEDs and stress sensors applications [1–4,13].

2 | EXPERIMENTAL

2.1 | Synthesis

$Sr_{(1-x)}Ga_2O_4$:xEu^{3+} (x = 0, 0.02, 0.05, 0.08, 0.09, 0.10 or 2, 5, 8, 9, and 10 mol%) phosphors were prepared using the traditional solid-state reaction approach. High-purity $SrCO_3$(99.9% purity), Ga_2O_3 (99.9% purity) and Eu_2O_3 (99% purity) from Sigma Aldrich were used as raw materials. The chemicals were stoichiometrically weighed and mixed using an agate mortar and pestle for 2 h with distilled water as the medium. The dried powder was transferred into an alumina crucible and then calcined at 1250°C for 5 h at a heating rate of 10°C/min. The sample was naturally cooled to room temperature to obtain the final product. The calcined powder was then ground for characterization. The same process was repeated for different concentrations of Eu_2O_3 (x = 0, 0.02, 0.05, 0.08, 0.09, 0.10). The sample codes given for the synthesized phosphors were SGEu: 0, 0.02, 0.05, 0.08, 0.09, and 0.10, respectively.

2.2 | Characterization

The crystalline structure and phase purity of the synthesized phosphors were investigated using a X-ray diffraction (XRD) technique on powder samples using a Bruker AXS D8 Advanced X-ray diffractometer. The patterns were collected over 2Θ ranging from 10 to 80° with a step size of 0.01^0 and at a scanning rate of 4.0^0/min using λ = 1.54 Å. The morphological information about the phosphors was analyzed using a Nova NanoSEM 450 UoK field emission scanning electron microscope (FESEM; FEI, USA). Energy dispersive X-ray spectroscopic (EDAX) analysis was carried out using a Carl Zeiss EVO 18 Research microscope. The optical absorption of undoped and doped phosphors was measured using a PerkinElmer UV/VIS/NIR Spectrometer Lambda 950 in the 200–800 nm range. An indigenous setup that included a photomultiplier tube (PMT 931A) positioned

underneath the Lucite plate and coupled to a digital storage oscilloscope was used to conduct the ML study. The emission of light was excited by dropping a load of mass 100 g onto phosphor from different heights using a guiding cylinder without any irradiation. The digital storage oscilloscope observed the corresponding intensity of the ML peak in the glow curve. A Fluorolog Horiba fluorescence spectrophotometer with a monochromator and a xenon lamp was used to record the PL excitation and emission characteristics. An Hitachi F-7000 fluorescence spectrophotometer was used to verify the lifetime measurements (Hitachi, Tokyo, Japan).

3 | RESULTS AND DISCUSSION

3.1 | XRD

The XRD patterns of $Sr_{(1-x)}Ga_2O_4:xEu^{3+}$ ($x = 0$, 0.02, 0.05, 0.08, 0.09, 0.10) phosphors are displayed in Figure 1. The XRD patterns were well matched with the standard ICDD card no. (01-070-5915) and showed that synthesized phosphors exist in a single phase with a monoclinic structure. The cell parameters were a = 8.3920 Å, b = 9.0180 Å and c = 10.6970 Å with P21/c (14) space group. The effective ionic radii of Sr^{2+}, Ga^{3+} and Eu^{3+} ions were 1.18, 0.62 and 1.17 Å, respectively [13]. By comparing the ionic radii and valence state, Eu^{3+} ions were more suitable to occupy the Sr^{2+} ion site in the host matrix. Doping of Eu^{3+} ions did not induce any marked changes in the host lattice's peak position, relative intensities and crystal structure [1]. XRD pattern did not show any other impurity peaks or additional diffraction peaks. All the diffraction peaks and (hkl) planes of Eu^{3+}-doped phosphors matched well with the host phosphor and maintain its single phase and monoclinic structure [13–15]. Therefore it confirmed the successful incorporation of Eu^{3+} ions into the host lattice [13,14].

3.2 | Morphological studies

Figure 2a,b represents the FESEM images of undoped and $SrGa_2O_4$: 0.08 Eu^{3+} phosphors. The particles were agglomerated, and their size distribution ranged from 1 to 3 μm for undoped and 1 to 5 μm for Eu^{3+}-doped $SrGa_2O_4$ phosphors. The results revealed that the doping process did not significantly change the morphology and size of the synthesized phosphors [14].

EDAX was carried out for the determination of quantitative analysis of the undoped and $SrGa_2O_4$: 0.08 Eu^{3+} phosphors and is portrayed in Figure 2c,d. The Sr, Ga, O, and Eu peaks were confirmed by

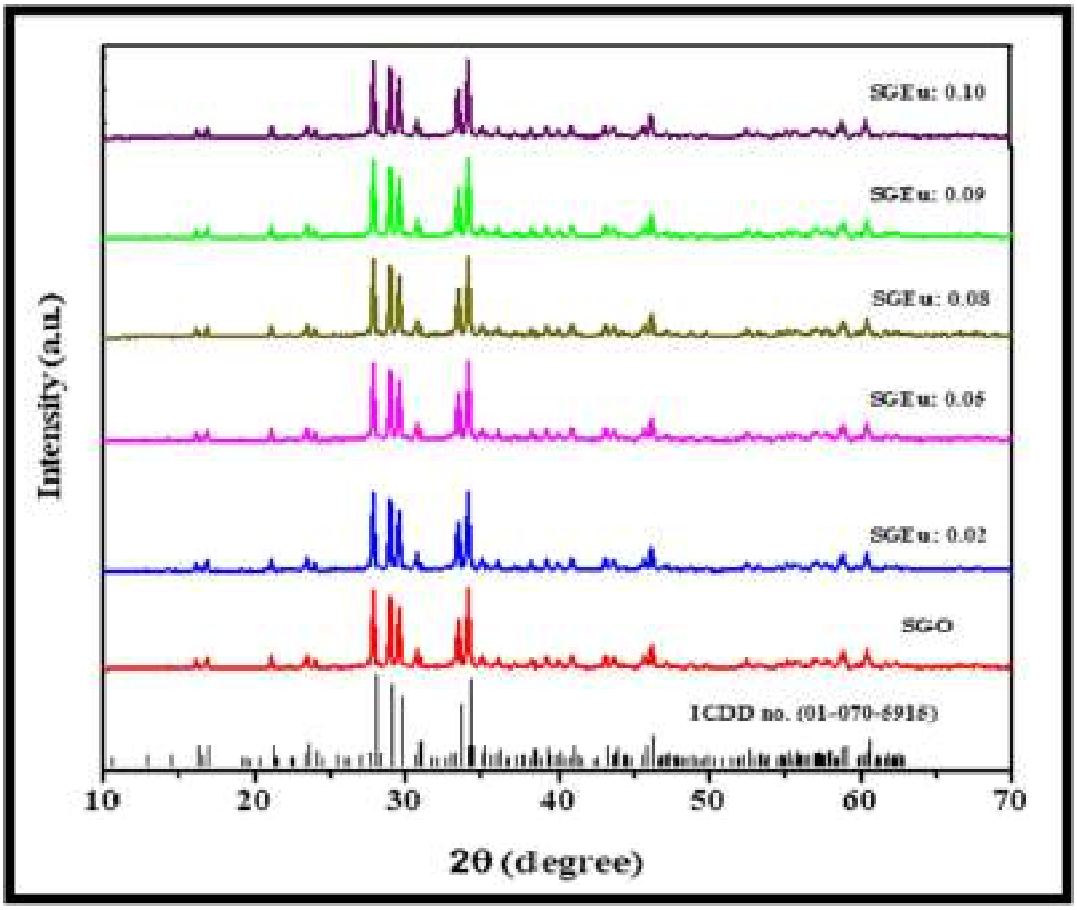

FIGURE 1 X-ray diffraction (XRD) patterns of $Sr_{(1-x)}Ga_2O_4:xEu^{3+}$ ($x = 0$, 0.02, 0.05, 0.08, 0.09, 0.10) phosphors.

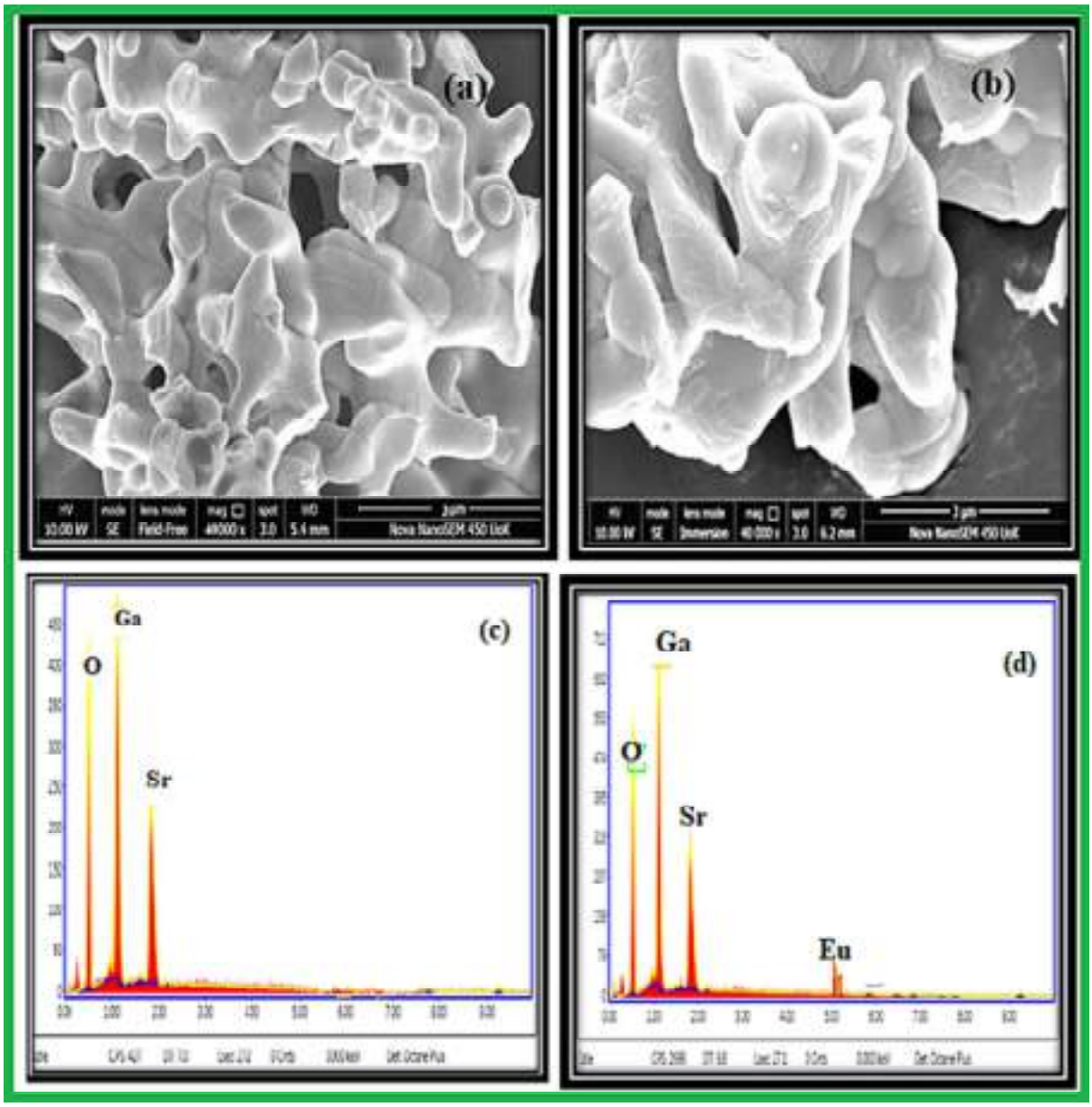

FIGURE 2 (a, b) Field emission scanning electron microscope (FESEM) images of $SrGa_2O_4$ and $SrGa_2O_4$: 0.08 Eu^{3+} phosphors. (c, d) Energy dispersive X-ray spectroscopic (EDAX) spectrum of $SrGa_2O_4$ and $SrGa_2O_4$: 0.08 Eu^{3+} phosphors.

the respective EDAX spectrum, which suggested the successful formation of synthesized phosphors [1,13]. The corresponding percentages of constituent elements are depicted in Table 1.

TABLE 1 Energy dispersive X-ray spectroscopic (EDAX) spectral analysis of $SrGa_2O_4$ and $SrGa_2O_4$: 0.08 Eu^{3+} phosphors.

	$SrGa_2O_4$ phosphor		$SrGa_2O_4$: 0.08 Eu^{3+} phosphor	
Elements	Weight %	Atomic %	Weight %	Atomic %
O K	20.06	53.14	31.22	68.86
GaL	65.96	40.10	41.53	21.02
SrL	13.98	6.76	22.26	8.97
Eu L	0	0	4.99	1.16
Total	100		100	

3.3 | UV–visible absorption spectra

The absorption spectra of undoped and Eu^{3+} doped $SrGa_2O_4$ phosphors are shown in Figure 3a. The maximum absorption recorded in the range below 300 nm was ascribed to the charge transfer band (CTB) [16]. The characteristic absorption peaks located at 365, 375, 395, 413, 465 and 534 nm corresponded to $^7F_0 \rightarrow {}^5D_4$, $^7F_0 \rightarrow {}^5L_8$, $^7F_0 \rightarrow {}^5L_6$, $^7F_0 \rightarrow {}^5D_3$, $^7F_0 \rightarrow {}^5D_2$ and $^7F_0 \rightarrow {}^5D_1$ transitions of Eu^{3+} ions, respectively, and it is clearly depicted in the inset of Figure 3a [17–19].

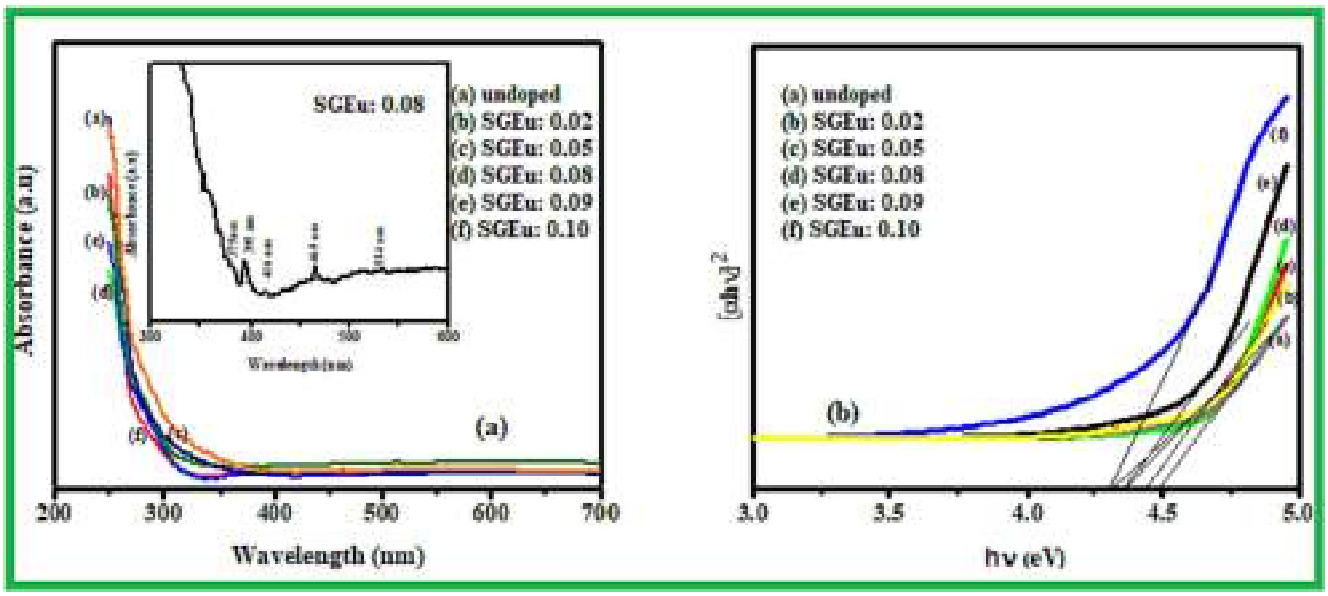

FIGURE 3 (a) Absorption spectra and (b) band-gap energies of $Sr_{(1-x)}Ga_2O_4:xEu^{3+}$ ($x = 0$, 0.02, 0.05, 0.08, 0.09, 0.10) phosphors.

Tauc's plots of $SrGa_2O_4$ and $SrGa_2O_4:xEu^{3+}$ phosphors are depicted in Figure 3b. The band-gap energies of these phosphors were calculated from Tauc's plot using Equation (1):

$$(\alpha h\nu)^{1/n} = c\,(h\nu - E_g) \tag{1}$$

where α is the absorption coefficient, and $h\nu$ is the photon energy. Direct transition is permitted if $n = 1/2$ and an indirect transition is permitted if $n = 2$. Calculation of the optical band gap involves extrapolating the linear portion of the curve to $(\alpha h\nu)^2 = 0$ of $(\alpha h\nu)^2$ versus the hv graph [20,21]. The direct band gap of the $SrGa_2O_4$ phosphor was found to be 4.48 eV. This indicates that $SrGa_2O_4$ is a wide band-gap semiconducting material [13]. The Ga^{3+} ions combined with UV-generated free electrons to produce oxygen vacancies. The band-gap energy decreased with an increase in the doping concentration of Eu^{3+} ions [13,14]. When europium ion was introduced into $SrGa_2O_4$ phosphor, CTB from the 2p orbit of O^{2-} to the 4f orbit of Eu^{3+} ion took place. A new level formed in the band gap between the conduction and valence bands [21]. If the doping density is high, Eu^{3+} states generate a band. If this band is extremely close to the conduction band edge, the band gap will narrow [16,17]. The band-gap energies were 4.43, 4.38, 4.32, 4.28 and 4.20 eV corresponding to $x = 0.02$, 0.05, 0.08, 0.09 and 0.10, respectively.

3.4 | ML study

The ML properties of undoped and Eu^{3+}-doped $SrGa_2O_4$ phosphors were investigated by a load of particular mass and shape dropped from different heights. The dependence of ML glow curve intensity with time for $Sr_{(1-x)}Ga_2O_4:xEu^{3+}$ ($x = 0.02$, 0.05, 0.08, 0.09, 0.10) phosphors at the height of 25 cm is shown in Figure 4a. In the present case, ML was excited impulsively, and a respective glow curve was formed due to the deformation of the powder sample [1]. The ML glow curve of the undoped phosphor consists of a single peak ascribed to some charge transfer that occurs during the mechanical process. Recombination occurs when a hole in the recombination centre combines with an electron in the conduction band [22–25]. Due to the deformation of the powder sample, an electric field is created in this mechanism, which ionizes either the electrons from the defect centre or the electrons from the valence band [2,3]. The electrons present in the conduction band then recombine with the holes in the luminescence centre. There will be a chance for these ions to get trapped for a particular time in the trapping levels present near the conduction band [4–6]. In certain alkali halides, the ML glow curve consists of two peaks. Among these, the first one corresponds to the recombination of electrons in the conduction band with holes in the valence band. The second delayed peak was reported to be due to the delayed trapping of the respective electron recombination with holes [26,27].

The ML glow curves of Eu^{3+}-doped $SrGa_2O_4$ phosphors also have a single peak with a drastic increase in the ML intensity. This single peak emission is associated with the deformation in the powder phosphors [23–26] and the recombination of electrons in the conduction band with holes in the luminescence centre [20–23]. The increase in the doping concentration of Eu^{3+} ions led to an increase in the concentration of electron–hole pairs generated during the ML process. The ML intensity increased with the increase in the concentration of Eu^{3+} ions and reached a maximum at $\boldsymbol{x} = 0.08$ (8 mol%); beyond that concentration the led to quenching of luminescence. The decrease in ML intensity at higher dopant concentrations may have been due to the decrease in the distance between the nearest free charge carriers. Effective energy transfer between free charge carriers causes a decrease in luminescence intensity [24]. The development of a

charged surface on the phosphor during fracture results in an increase in recombination luminescence. [28,29]. An electric field of 10^7–10^8 Vm^{-1} may be produced between oppositely charged surfaces. This field may cause the dielectric breakdown of the crystals, and the subsequent recombination of free carriers gives rise to recombination luminescence [10]. The variation in ML glow curve intensity with Eu^{3+} concentration is shown in Figure 4b.

The same procedure was used when dropping the same load from various heights. Figure 5a represents the variation in the ML intensity of $SrGa_2O_4$: 0.08 Eu^{3+} phosphor with falling heights of 10, 15, 20 and 25 cm, respectively. A sharp and single narrow peak was recorded for different falling heights. ML intensity increased with an increase in falling height, and maximum intensity was achieved at 25 cm. As the impact height was increased, the area of the fractured charged surface also increased, which enhanced the recombination luminescence [6,11]. As the height was increased the sharpness of the peak increased.

Figure 5b represents the dependence of ML peak intensity of $SrGa_2O_4$: 0.08 Eu^{3+} phosphor with different impact velocities. The impact velocity $v = (2gh)^{1/2}$, where g is the acceleration due to gravity and ***h*** is the height through which the load was dropped freely [30,31]. The intensity of the single peak in the ML glow curve increased with the increase in the impact velocity from 196 to 490 cm/s, respectively. The phosphor is increasingly compressed with the increase in impact velocity [25–27]. When the load strikes the phosphor, a positive charge is built on one of the newly created surfaces, and a negative charge develops on the other cracked surface of the same phosphor. These charged particles produced an electric field that emitted electrons from the negatively charged surface and had an effect on the positively charged surface [29]. Therefore, luminous centres will be able to accommodate more electrons that recombine with holes already existing in the recombination centre. Such recombination of carriers acts as a source for the production of ML emissions [30–32]. The de-excitation of Eu^{3+} ions from excited energy levels to

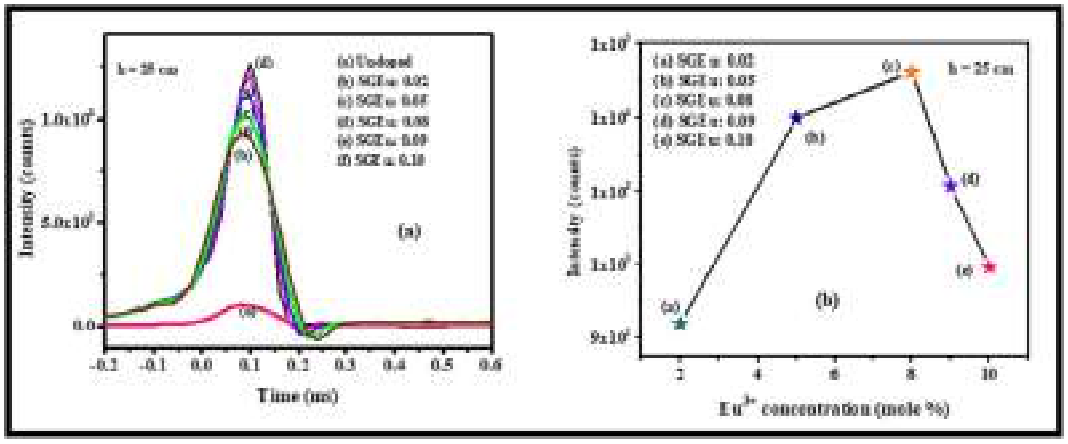

FIGURE 4 (a) Variation in mechanoluminescence (ML) intensity versus time of $Sr_{(1-x)}Ga_2O_4$:xEu^{3+} ($x = 0$, 0.02, 0.05, 0.08, 0.09, 0.10) phosphors. (b) Variation of ML peak intensity with Eu^{3+} concentration in $SrGa_2O_4$ phosphors.

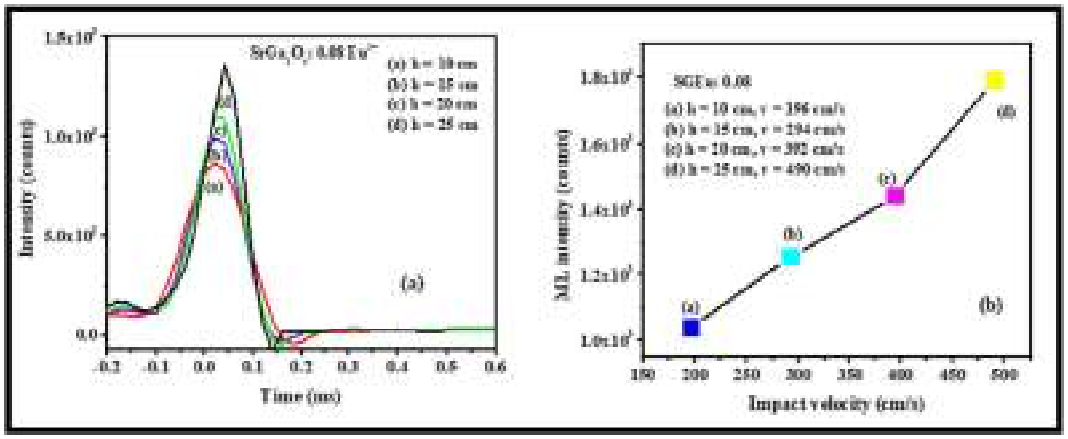

FIGURE 5 (a) Variation of mechanoluminescence (ML) intensity of $SrGa_2O_4$: 0.08 Eu^{3+} phosphor with different heights. (b) Impact velocity dependence of total ML intensity of $SrGa_2O_4$: 0.08 Eu^{3+} phosphors.

their ground state is also a reason for the increase in the intensity of ML emission. Therefore, ML emission can linearly increase with falling height and impact velocity [32–34]. The ML studies indicate that the synthesized phosphors may have applications in stress detectors and sensors [27,29–31].

3.5 | PL studies of $SrGa_2O_4$ phosphor

PL is the ability of a material to absorb photons of required energy and then re-radiate the photons with lower energy. The excitation and emission spectrum of $SrGa_2O_4$ phosphor is depicted in Figure 6. The excitation peak at 225 nm (inset of Figure 6) arose mainly from the host absorption and the $O^{2-} \rightarrow Ga^{3+}$ charge transfer transitions, respectively [15]. The self-activated broad blue emission with maximum intensity at 420 nm was due to the presence of Ga^{3+} ions in the octahedrally coordinated site and could act as a luminescence centre in the host material [13,15]. The electronic transition from the excited energy levels $^4T_{2B}$, $^4T_1$, $^4T_{2A}$ and ^2E_B to the ground state $^4A_2$ of Ga ion gave blue emission [13–15].

3.5.1 | PL spectra of $SrGa_2O_4$:xEu^{3+} phosphors

The PL excitation and emission spectra were collected for the various concentrations of Eu^{3+} ions to explore the impact of the doping concentration of Eu^{3+} on the luminescence properties of the $SrGa_2O_4$ phosphor. The PL excitation spectrum of $SrGa_2O_4$: 0.08 Eu^{3+} phosphor monitored at 616 nm is shown in Figure 7a. An electron's excitation from the delocalized 2p orbital of the O^{2-} to the unoccupied 4f orbital of the Eu^{3+} ion causes the CTB to have a wavelength in the range of 200–350 nm [35–37]. Beyond CTB, the characteristic excitation peaks of Eu^{3+} ions designated at 362, 374, 382, 394, 413, 464, 525 and 532 nm were attributed to the Eu^{3+} ion transitions at $^7F_0 \rightarrow {}^5D_4$, $^7F_0 \rightarrow {}^5L_7$, $^7F_0 \rightarrow {}^5G_2$, $^7F_0 \rightarrow {}^5L_6$, $^7F_0 \rightarrow {}^5D_3$, $^7F_0 \rightarrow 5D_2$, $^7F_0 \rightarrow {}^5D_1$, respectively [38,39]. These peaks arose due to the intra 4f-4f transitions of Eu^{3+} ions. The most intense peak was recorded at 394 nm corresponding to the $^7F_0 \rightarrow {}^5L_6$ transition of the Eu^{3+} ions. This shows that NUV chips are an efficient way to activate these phosphors. The intensity of excitation peaks increased up to $x = 0.08$ and beyond that the limit the intensity tended to decrease. These excitation peaks indicated that phosphors with Eu^{3+} doping can emit red light in the visible range [40–42].

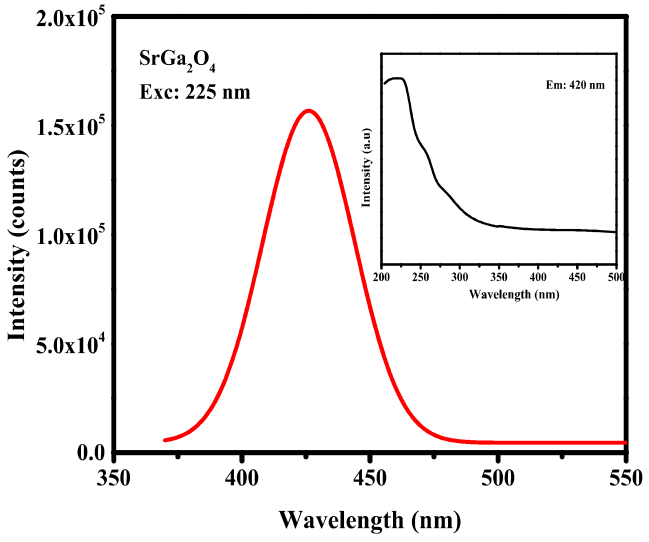

FIGURE 6 Emission spectrum of $SrGa_2O_4$ phosphor.

Figure 7b represents the emission spectra of Eu^{3+}doped $SrGa_2O_4$ phosphors excited at 395 nm. The spectra consisted of sharp characteristic emission peaks of Eu^{3+}ions in the 550–750 nm range ascribed to the $^5D_0 \rightarrow {}^7F_j$ ($j = 0, 1, 2, 3$) transitions [38,40–42]. The prominent peaks were assigned at 577 ($^5D_0 \rightarrow {}^7F_0$), 587 ($^5D_0 \rightarrow {}^7F_1$), 598 ($^5D_0 \rightarrow {}^7F_1$), 616 ($^5D_0 \rightarrow {}^7F_2$), 645 ($^5D_0 \rightarrow {}^7F_3$) and 654 nm ($^5D_0 \rightarrow {}^7F_3$), respectively [43–45]. The most intense emission was credited to the hypersensitive forced ED $^5D_0 \rightarrow {}^7F_2$ transition of Eu^{3+} ions at 616 nm. The luminescence emission intensity at 616 nm was stronger than that at 598 nm (magnetic dipole [MD] transition), which points out that the Eu^{3+} ion is located at the site without inversion symmetry in the host lattice [42–44]. The ED transitions strongly depend on the local environment of ligands and therefore such transitions are hypersensitive in nature. The ED transition favours when activator ions occupy the site without inversion symmetry and it provides red emission for the phosphors. At the same time, MD transitions are independent of the environment of ligand ions and such transitions favour when an activator ion occupies the site with an inversion centre and it gives orange–red emission for a material. The emission peaks formed due to $^5D_0 \rightarrow {}^7F_2$ and $^5D_0 \rightarrow {}^7F_1$ transitions provide red and orange–red emissions for the phosphors [44–46]. The f–f transitions of Eu^{3+} ions were not significantly affected by the ligands ions because of the shielding effect of the valence electron of the Eu^{3+} ions from 5s and 5p outer electrons. Therefore emission spectra showed the same spectral arrangement for different concentrations of Eu^{3+} ions and differed only in their emission intensities. The emission at 616 nm significantly increased with Eu^{3+} concentration, and maximum intensity was achieved for $x = 0.08$ (8 mol%). Transcending that level, concentration quenching takes place. Higher dopant concentrations cause the Eu^{3+} ions to move closer to one another by shortening the space between them. Some of the activator Eu^{3+} ions could not reach the sites of Sr^{2+} ions; in this case, nonradiative energy transfer is stronger than ordinary light emission. Therefore, luminescence intensity decreased for higher doping concentrations [41,42]. The resonant energy transfer became stronger, which enhanced the non-radiative relaxation. Therefore it causes a decrease in the PL intensity of the host.

Figure 7c shows the variation in PL intensity at 616 nm with various doping concentrations of Eu^{3+} ions excited at 395 nm. ML glow curve intensity's dependence on Eu^{3+} concentration is consistent with the PL result. In both cases, maximum intensity has been noted when $x = 0.08$. There is no change in the appearance of the ML glow curve

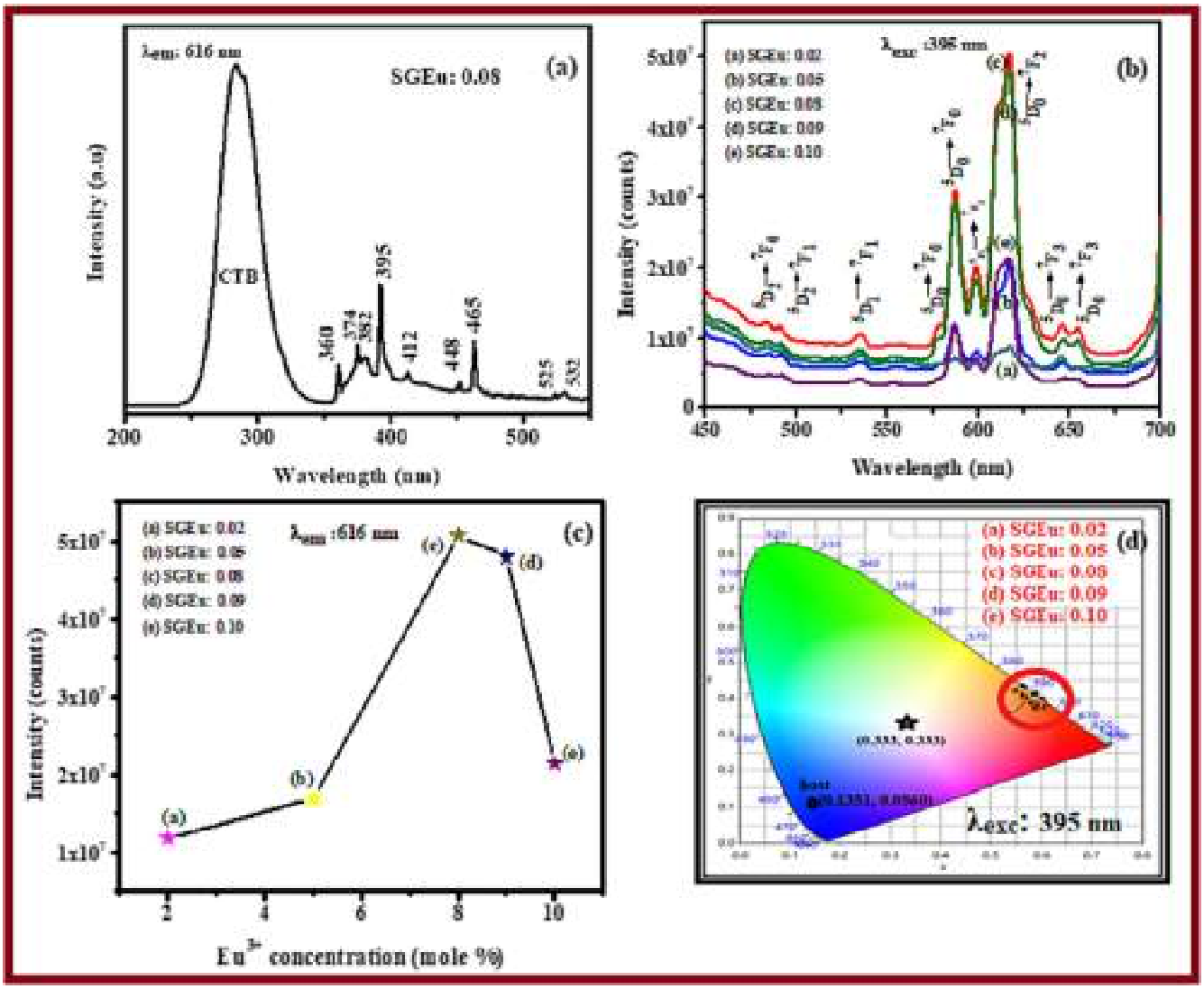

FIGURE 7 (a) Excitation spectrum of $SrGa_2O_4$: 0.08 Eu^{3+} phosphor. (b) Emission spectra of $Sr_{(1-x)}Ga_2O_4$:xEu^{3+} (x = 0, 0.02, 0.05, 0.08, 0.09, 0.10) phosphors. (c) Variation in photoluminescence (PL) emission intensity with different doping concentrations of Eu^{3+} ions attributed to $^7F_0 \rightarrow {}^5D_2$ transitions under the excitation of 395 nm. (d) CIE chromaticity diagram of $Sr_{(1-x)}Ga_2O_4$:xEu^{3+} (x = 0, 0.02, 0.05, 0.08, 0.09, 0.10) phosphors excited at 395 nm.

and PL emission spectra for different concentrations of Eu^{3+} ions. The maximum intensity is attained for smaller concentrations of activator ions. Such results indicate the benefit of these phosphors with less cost in radiation dosimetry and phosphor-converted WLED applications [35,39,41].

The quenching of luminescence can be described based on different interactions that favour the nonradiative energy transfer mechanism in the phosphors. It includes exchange interactions, multipolar interaction and radiation re-absorption [40]. The interaction allowed in the phosphors depended on the value of critical distance r_c between the two nearest Eu^{3+} ions. The critical distance is the minimum distance between the activator ions and quenching centres in the phosphor lattice, and can be determined using the relation given in Equation (2):

$$r_c = 2\left(\frac{3V}{4\pi XcN}\right)^{1/3} \quad (2)$$

where r_c is the critical distance between the dopant ion and quenching centre, V is the volume of the unit cell of the host lattice, X_c is the critical concentration of the dopant ions after which concentration quenching takes place and N is the number of host cations in the unit cell [39]. If the critical distance is below 5 Å, exchange interactions are stronger, and if the value is greater than 5 Å, multipolar interaction becomes more prominent [47]. In the present work, V = 802.77 Å^3, N = 8 and X_c = 0.08 for the $SrGa_2O_4$ host lattice. The critical distance was calculated to be 13.4 Å, which is larger than 5 Å. As a result, electric multipolar interaction governs concentration quenching in the $SrGa_2O_4$:Eu^{3+} phosphors.

The quantum efficiency of the $SrGa_2O_4$: 0.08 Eu^{3+} phosphor excited at 395 nm is 12.68%. Quantum efficiencies for the commercially available Y_2O_3:Eu^{3+} and Y_2O_2S:Eu^{3+} red phosphors are 9.6% and 4.2%, respectively under the excitation of 395 nm [39–41]. The quantum efficiency of the synthesized phosphor is higher than that of commercial red phosphors. This indicates that Eu^{3+}-doped $SrGa_2O_4$ phosphor can be a candidate for red emitter in phosphor-converted WLEDs.

The asymmetric ratio (R) is significant for predicting the local symmetry of Eu^{3+} ions and gives information about the asymmetric nature in the neighbourhood of Eu^{3+} ions. It can be calculated by the ratio of the integral intensity of the ED transition to the MD transition [47]:

$$R_{21} = \frac{\int I_2\, {}^5_0D \rightarrow {}^2_7F \; d\lambda}{\int I_1\, {}^5_0D \rightarrow {}^1_7F \; d\lambda} \tag{3}$$

where I_1 and I_2 denote the integral intensities for the Eu^{3+} transitions $^5D_0 \rightarrow {}^7F_1$ (585–600 nm) and $^5D_0 \rightarrow {}^7F_2$ (605–640 nm), respectively. It is clear from the emission spectra that ED transition $^5D_0 \rightarrow {}^7F_2$ is more predominant than MD transition $^5D_0 \rightarrow {}^7F_1$. If the asymmetry ratio is less than 1, this demonstrates the predominance of the MD $^5D_0 \rightarrow {}^7F_1$ transition, whereas if the value is greater than 1, then it shows the predominance of ED $^5D_0 \rightarrow {}^7F_2$ transitions of Eu^{3+} ions [48]. In the present case, the value of R lies in the range 1.237–2.501, indicating that Eu^{3+} ions are located at the site without inversion symmetry or higher asymmetry in the host lattice [49]. The asymmetric ratio increases with Eu^{3+} dopant concentration up to 0.08 and, beyond that concentration limit, the value of R decreased with an increase in dopant concentration due to concentration quenching.

3.5.2 | Colour characteristics

The colour chromaticity diagram of $SrGa_2O_4$:Eu^{3+}phosphors excited at 395 nm is shown in Figure 7d. The undoped $SrGa_2O_4$ phosphor shows blue emission with colour coordinates (0.1351, 0.086) and that of $SrGa_2O_4$: 0.08 Eu^{3+} phosphor falls in the red region with coordinates (0.6102, 0.3810), respectively. The colour of the host phosphor is shifted from blue to red region after the incorporation of Eu^{3+} ions. The obtained colour coordinate is consistent with the standard red coordinates (0.670, 0.33). Therefore Eu^{3+}-doped $SrGa_2O_4$ phosphors can be excited with UV or near-UV light as a source and have practical applications in the field of UV or NUV LEDs and display devices [50–52].

The colour purity of the synthesized phosphors ranged from 92.4% to 97.6%, with maximum colour purity (97.6%) obtained for the $SrGa_2O_4$: 0.08 Eu^{3+} phosphor. The synthesized phosphors have better colour purity, indicating the phosphor capability in red-emitting and solid-state light-emitting device applications [48,49].

TABLE 2 CIE, colour purity and correlated colour temperature (CCT) of $Sr_{(1-x)}Ga_2O_4$:xEu^{3+} ($x = 0$, 0.02, 0.05, 0.08, 0.09, 0.10) phosphors excited at 395 nm.

	CIE coordinates			
Sample code	x	y	CCT (K)	Colour purity (%)
SGEu:0.02	0.5678	0.4312	1801	92.4
SGEu:0.05	0.5992	0.4001	1464	96.0
SGEu:0.08	0.6102	0.3810	1324	97.6
SGEu:0.09	0.6078	0.3921	1365	95.3
SGEu:0.10	0.6009	0.3984	1447	94.5

Correlated colour temperature (CCT) is another critical parameter for verifying the efficiency of the phosphors, and it specifies the colour temperature of the light emitted from the synthesized phosphors in Kelvin (K) [46,53]. The CCT values of the $Sr_{(1-x)}Ga_2O_4$:**x**Eu^{3+} (**x** = 0.02, 0.05, 0.08, 0.09, 0.10) phosphors lay in the 1300–1900 K range revealed the warmer orange–red light emission from the phosphors and this result was consistent with the Commission Internationale de l'éclairage (CIE) coordinates [54,55]. Generally, warm white light used for domestic purposes was preferred to CCT at less than 5000 K [56]. The obtained CCT values showed the applicability of the synthesized Eu^{3+}-doped $SrGa_2O_4$ phosphors for the purpose of red light in domestic lighting appliances [45,47]. Table 2 lists the colour coordinates, colour purity, and CCT of synthesized phosphors.

3.5.3 | Lifetime measurements

Lifetime measurement is used to study the luminescence characteristics of phosphors. The term lifetime indicates the time in which the intensity of a single emission peak becomes 1/e of the original intensity [38]. Figure 8a–d shows the decay curves of Eu^{3+}-activated $SrGa_2O_4$ phosphors excited by 394 nm, corresponding to the emission wavelength of 616 nm. The faster decay rate shows the influence of the f–f transition in Eu^{3+} ions present in the host lattice. The luminescence lifetime decay curve can be fitted with the exponential function. The decay time corresponding to the particular excitation was calculated using the principle of the exponential formula:

$$I = A_1 exp\,(-t/\tau_1) + A_2 exp\,(-t/\tau_2) \tag{4}$$

where I is phosphorescence intensity, A_1 and A_2 are constants, t is time, and $\boldsymbol{\tau_1}$ and $\boldsymbol{\tau_2}$ are decay times for the exponential components [41,54]. In this particular study, the decay dynamics at 616 nm was bi-exponential for Eu^{3+}-doped $SrGa_2O_4$ phosphors. The initial intensity underwent very fast decaying, and further decaying took place very slowly [38,39,46]. The lifetimes of the phosphors were determined from the time versus intensity graph. From the graph, the value of $\tau_1 = 0.746$ ms and $\tau_2 = 0.301$ ms, $\tau_1 = 0.735$ ms and $\tau_2 = 0.293$ ms, $\tau_1 = 0.612$ ms and $\tau_2 = 0.213$ ms and $\tau_1 = 0.322$ ms and $\tau_2 = 0.743$ ms were for $x = 0.02$, 0.05, 0.08, 0.10, respectively [35].

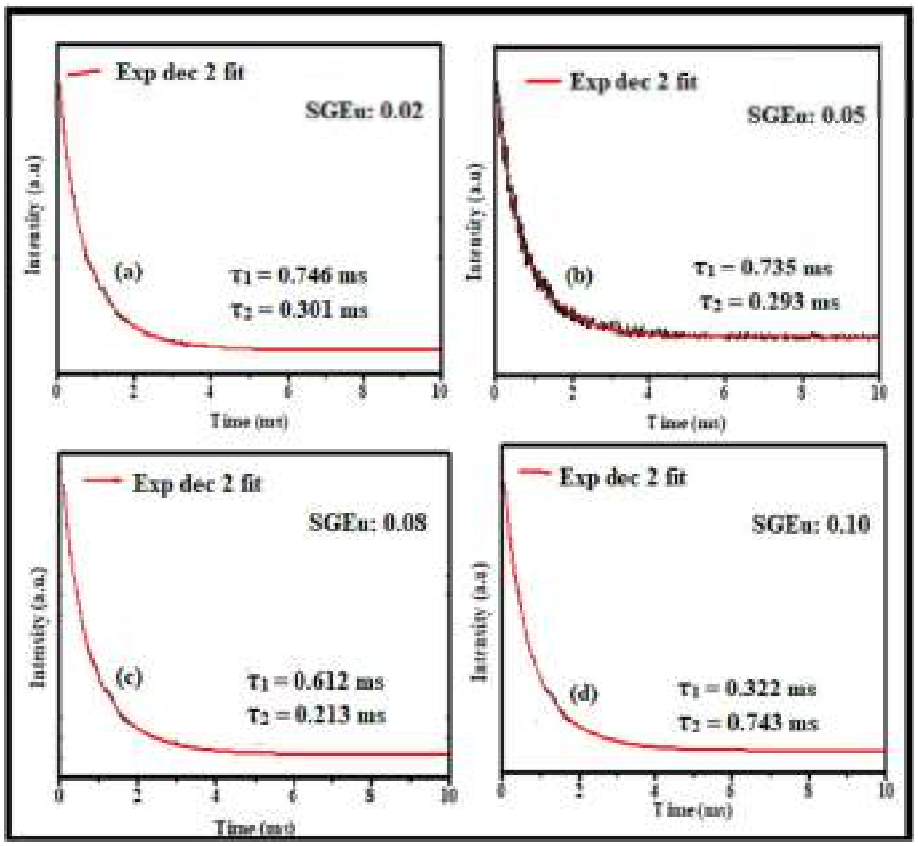

FIGURE 8 (a–d) Lifetime measurement of $Sr_{(1-x)}Ga_2O_4:xEu^{3+}$ ($x = 0.02, 0.05, 0.08, 0.10$) phosphors.

4 | CONCLUSION

A series of $SrGa_2O_4:Eu^{3+}$ red-emitting phosphors were synthesized using a solid-state reaction method. The structure, microstructure, optical and luminescence properties of undoped and Eu^{3+}-doped phosphors were investigated. XRD analysis showed that these phosphors are single phase with a monoclinic structure. The ML glow curve had a single peak that was mostly obtained due to deformation caused by the impact of the load. The recombination of holes and electrons produced the ML emission in the recombination centre in the conduction band. The magnitude of the ML glow curve varied linearly with impact velocity and increased with increasing Eu^{3+} ion concentration up to the optimal concentration. The $SrGa_2O_4$ exhibited self-activated blue emission at 420 nm due to the presence of Ga^{3+} ions in the octahedrally coordinated site. $SrGa_2O_4:Eu^{3+}$ phosphors could be effectively excited at 395 nm, and it showed better red emission in the 550–700 nm range ascribed to the $^5D_0 \rightarrow {}^7F_j$ ($j = 1$–4) transition of the Eu^{3+} ion. The hypersensitive ED transition was more dominant than the MD transition and was confirmed by the asymmetric ratio and critical distance calculations of the synthesized phosphors. The $SrGa_2O_4:Eu^{3+}$phosphor could be efficiently excited by near-UV and UV light as sources and could exhibit better quality red light at 616 nm ascribed to the $^5D_0 \rightarrow {}^7F_2$ transition of Eu^{3+} ions. The CIE coordinates and colour purity of the $SrGa_2O_4$: 0.08 Eu^{3+} phosphor were calculated to be (0.6102, 0.3810) and 97.6%, respectively. The warm orange–red light emission from the phosphors was revealed by the CCT values of synthesized phosphors. The quantum efficiency was found to be 12.68%, which was higher than that of the commercially available red phosphors. In the present study, all Eu^{3+}-doped phosphors exhibited both ML and PL emissions originating from the same activator Eu^{3+} ions. Both in ML and PL, the maximum emission was achieved for the concentration at $x = 0.08$. From the ML and PL studies, $SrGa_2O_4:xEu^{3+}$ phosphors showed excellent luminescence properties. Therefore, the synthesized phosphors could be used as suitable components in stress sensors, UV–NUV LEDs, and solid-state light-emitting devices.

AUTHOR CONTRIBUTIONS

Baby Vasanthi: Conceptualization; formal analysis; investigation; writing—original draft; visualization; writing—review and editing. **Narayana Panickar Gopakumar:** Conceptualization; supervision; writing—review and editing. **Prabhakaran Sreekumari Anjana:** Conceptualization; validation; supervision; writing—revew and editing. **Girija Nair:** Writing—review and editing. **Baby Vasanthi, Narayana Panickar Gopakumar, Prabhakaran Sreekumari Anjana, and Girija Nair:** Approval of the version of the manuscript.

ACKNOWLEDGEMENTS

The authors are thankful to the Department of Physics, University of Kerala, Kariavattom, for the XRD analysis. The authors are grateful to the Department of Optoelectronics, University of Kerala, Kariavattom Campus, for FESEM, UV–visible, and PL measurements. The authors

are grateful to CLIF, University of Kerala, for EDAX, quantum efficiency, and decay studies. One of the authors is thankful to the Directorate of Collegiate Education, Kerala, for granting the ASPIRE Fellowship for the successful completion of this work.

CONFLICT OF INTEREST STATEMENT

There are no conflicts to declare.

DATA AVAILABILITY STATEMENT

Research data are not shared.

ORCID

Prabhakaran Sreekumari Anjana https://orcid.org/0000-0003-4610-1918

REFERENCES

[1] B. Vasanthi, N. Gopakumar, P. S. Anjana, *J. Lumin.* **2022**, *241*, 118486.
[2] S. J. Sajan, N. Gopakumar, P. S. Anjana, K. Madhukumar, *J. Lumin.* **2016**, *174*, 11.
[3] J.-C. Zhang, C.-N. Xu, X. Wang, Y.-Z. Long, *J. Adv. Dielectr.* **2014**, *4*(3), 1430003.
[4] Y.-L. Yang, T. Li, F. Guo, J.-Y. Yuan, C.-H. Zhang, Y. Zhou, Q.-L. Li, D.-Y. Wan, J.-T. Zhao, Z.-J. Zhang, *Inorg. Chem.* **2022**, *61*(10), 4302.
[5] B. P. Chandra, R. N. Baghel, A. K. Luka, T. R. Sanodiya, R. K. Kuraria, S. R. Kurari, *J. Lumin.* **2009**, *129*, 760.
[6] M. R. Revupriya, P. S. Anjana, N. Gopakumar, M. S. Anju, *Mater. Res. Express* **2020**, *7*, 026203.
[7] P. Jha, A. Kharea, *J. Alloys Compd.* **2020**, *847*, 156428.
[8] S. J. Sajan, N. Gopakumar, P. S. Anjana, R. S. Kher, M. R. Revupriya, *Optik* **2018**, *156*, 921.
[9] A. Kharea, B. N. Bhargavi, N. Chauhan, N. Brahme, *Optik* **2014**, *125*, 4655.
[10] M. Saleem, R. Neema, M. Mittal, P. K. Sharma, *Int. J. Sci. Res. Phys. Appl. Sci.* **2015**, *3*(3), 4.
[11] M. Dubernet, Y. Gueguen, P. Houizot, F. Célarié, J. C. Sangleboeuf, H. Orain, T. Rouel, *Appl. Phys. Lett.* **2015**, *107*, 151906.
[12] R. Shrivastava, J. Kaur, *J. Radiat. Res. Appl. Sci.* **2015**, *8*, 201.
[13] X. Cai, Z. Mu, S. Zhang, D. Zhu, Q. Wang, Y. Yang, D. Luo, F. Wu, *J. Lumin.* **2018**, *200*, 169.
[14] M. Ayvacıklı, A. Ege, S. Yerci, N. Can, *J. Lumin.* **2011**, *131*, 2432.
[15] B. C. Jamalaiah, M. Jayasimhadri, *J. Mol. Struct.* **2019**, *1178*(5), 394.
[16] K. R. Ashwini, H. B. Premkumar, G. P. Darshan, R. B. Basavaraj, H. Nagabhushana, B. Daruka Prasad, *Sci. Adv. Mater. Dev.* **2020**, *5*, 111.
[17] P. J. Chaware, K. G. Rewatkar, *Int. J. Chem. Math. Phys.* **2021**, *5*, 1.
[18] A. De, A. K. Dey, B. Samanta, U. K. Ghorai, *J. Mater. Sci. Mater. Electron* **2021**, *32*, 8648.
[19] J. F. Wang, H. Zu, C. W. Lin, S. J. Ding, P. Y. Shao, Y. Xia, *Int. J. Opt.* **2020**, *2020*, 5.
[20] A. Ghosh, S. Bhattacharya, A. Shosh, *J. Appl. Phys.* **2007**, *101*, 083511.
[21] R. Raji, R. G. Abhilash Kumar, K. G. Gopchandran, *J. Lumin.* **2019**, *205*, 179.
[22] G. Tiwari, N. Brahme, R. Sharma, D. P. Bisen, S. K. Sao, A. Kharea, *J. Lumin.* **2017**, *183*, 89.
[23] N. Tiwari, R. K. Tsmrakar, *J. Radiat. Res. Appl. Sci.* **2015**, *8*, 68.
[24] S. K. Sao, N. Brahme, D. P. Bisen, G. Tiwari, *Phys. Procedia* **2015**, *76*, 59.
[25] H. Chen, L. Wu, T. Sun, R. Dong, Z. Zheng, Y. Kong, Y. Zhang, J. Xu, *Appl. Phys. Lett.* **2020**, *116*, 051904.
[26] H. Trabelsi, M. Akl, S. H. Akl, *Powder Technol.* **2021**, *384*, 70.
[27] J. Grigorjevaite, A. Katelnikovas, *ACS Appl. Mater. Interfaces* **2016**, *8*, 3177.
[28] H. Liu, L. Yu, F. Li, *J. Phys. Chem. Solids* **2013**, *74*, 196.
[29] T. Cai, S. Guo, Y. Li, D. Peng, X. Zhao, Y. Liu, *Rev. Sci. Instrum.* **2018**, *89*, 045006.
[30] A. K. Upadhyay, S. J. Dhoble, R. S. Kher, *Luminescence* **2011**, *26*(6), 471.
[31] R. Sharma, D. P. Bisen, S. J. Dhoble, N. Brahme, B. P. Chandra, *J. Lumin.* **2011**, *131*, 2089.
[32] B. P. Chandra, V. D. Sonwane, B. K. Haldar, S. Pandey, *Opt. Mater.* **2011**, *33*, 444.
[33] M. R. Kadukar, P. W. Yawalkar, R. Choithranic, S. J. Dhoble, *Luminescence* **2015**, *30*(8), 1219.
[34] S. Sailaja, S. J. Dhoble, N. Brahme, B. S. Reddy, *J. Mater. Sci.* **2011**, *46*, 7793.
[35] M. Rai, S. K. Singh, K. Mishra, R. Shankar, R. K. Srivastava, S. B. Rai, *J. Mater. Chem.* **2014**, *2*, 7918.
[36] J. Singh, J. Manam, *J. Mater. Sci.* **2016**, *51*, 2886.
[37] C. Y. Lin, S. H. Yang, J. L. Lin, C. F. Yang, *Appl. Sci.* **2017**, *7*, 30.
[38] S. H. Lee, J. S. Yu, *Mater. Res. Bull.* **2014**, *50*, 354.
[39] M. Vasile, P. Vlazan, N. Avram, *J. Alloys Compd.* **2010**, *500*, 185.
[40] J. Liang, P. Du, H. Guo, L. Sun, B. Li, X. Huang, *Dyes Pigm.* **2018**, *157*, 40.
[41] J. Lu, Z. Mu, D. Zhu, Q. Wang, F. Wu, *J. Lumin.* **2018**, *196*, 50.
[42] M. Liao, Z. Mu, S. Zhang, F. Wu, Z. Nie, Z. Zheng, X. Feng, Q. Zhang, J. Feng, D. Zhu, *J. Lumin.* **2019**, *210*, 202.
[43] I. P. Sahu, D. P. Bisen, N. Brahme, R. K. Tamrakar, *J. Radiat. Res. Appl. Sci.* **2015**, *8*, 104.
[44] I. P. Sahu, D. P. Bisen, R. K. Tamrakar, K. V. R. Murthy, M. Mohapatra, *J. Sci. Adv. Mater. Devices* **2017**, *2*, 69.
[45] J. Grigorjevaite, E. Ezerskyte, A. Minderyte, S. Stanionyte, R. Juskenas, S. Sakirzanovas, A. Katelnikovas, *Materials* **2019**, *12*, 3275.
[46] Q. Bin, T. Zilong, Z. Zhongtai, *J. Rare Earths* **2007**, *25*, 286.
[47] E. Rai, R. S. Yadav, D. Kumar, A. K. Singh, V. J. Fulari, S. B. Rai, *Spectrochim. Acta A Mol. Biomol. Spectrosc.* **2020**, *243*, 118787.
[48] V. Dubey, J. Kaur, S. Agrawal, N. S. Suryanarayana, K. V. R. Murthy, *Optik* **2013**, *124*, 5585.
[49] C. H. Moon, S. K. Singh, D. G. Lee, S. S. Yi, K. Jang, *Ceram. Int.* **2012**, *38*(8), 6789.
[50] P. Du, J. S. Yu, *Appl. Phys. A: Mater. Sci. Process.* **2019**, *2*, 125.
[51] I. E. Kolesnikov, A. V. Povolotskiy, D. V. Mamonova, E. Yu. Kolesnikov, A. V. Kurochkin, E. Lähderanta, M. D. Mikhailov, *J. Eare Earths* **2018**, *36*(5), 474.
[52] Y. V. Baklanova, L. G. Maksimova, O. A. Lipina, A. P. Tyutyunnik, A. Y. Chufarov, V. G. Zubkov, *Mater. Res. Express* **2019**, *6*, 6.
[53] S. C. Lal, A. M. Aiswarya, K. S. Sibi, G. Subodh, *J. Alloys. Compd.* **2019**, *788*, 1300.
[54] X. Zhu, Y. P. Pu, X. Pu, X. Xie, M. Liu, Q. Lu, *Mater. Lett.* **2019**, *253*, 21.
[55] I. E. Kolesnikov, R. S. Bubnov, A. V. Povolotskiy, Y. P. Biryukov, A. V. Povolotckaia, O. Yu Shorets, S. K. Filatov, *Ceram. Int.* **2021**, *47*(6), 8030.
[56] S. Yildirim, S. Demirci, K. Ertekin, E. Celik, Z. A. Alicikus, *J. Adv. Ceram.* **2017**, *6*(1), 33.

How to cite this article: B. Vasanthi, N. P. Gopakumar, P. S. Anjana, G. Nair, *Luminescence* **2023**, 1. https://doi.org/10.1002/bio.4602